A New Actuator Surface Model with Improved Wake Model for CFD Simulations of Rotorcraft

Daniel Linton
PhD Student
The University of Sydney
Sydney, Australia

George Barakos
Professor
The University of Glasgow
Glasgow, United Kingdom

Ronny Widjaja
Science Team Leader
The Defence Science and Technology Group
Melbourne, Australia

Ben Thornber
Associate Professor
The University of Sydney
Sydney, Australia

ABSTRACT

Simulations of rotorcraft operating in unsteady flow-fields, manoeuvring flight, or with complex rotor configurations pose a significant challenge to current simulation methods. Simplified rotor models lack the generality required for the diverse range of operating conditions that a rotor may be exposed to, while higher-fidelity Navier-Stokes CFD simulations with fully-resolved rotors are expensive in terms of computational resources, simulation time, and pre-processing time. Here we present a new rotor and wake model which is fully-coupled to a CFD solver and is based on the actuator surface model. This model is designed to reduce the cost of complex rotorcraft simulations in comparison with fully-resolved simulations and provide greater generality than other rotor models. Results from simulations using the new actuator surface and wake model provide validation of the concept for hover and forward flight. The spanwise loading distribution, thrust coefficient, and wake geometry are shown to be reasonable in comparison with data from experiments, fully-resolved simulations, and prescribed wake models.

INTRODUCTION

Complex rotorcraft simulations are becoming more common because of the need to analyse the performance and handling of rotorcraft in situations where aerodynamic interactions due to the presence of other bodies and rotors are of importance. Such simulations include operational scenarios involving multiple rotorcraft, or operations in confined spaces such as around natural or urban terrain (Ref. 1), ships (Refs. 2, 3), or oil-rigs (Ref. 4). Other examples of complex rotorcraft simulations are those of multi-rotor, compound rotorcraft, and vehicles with side-by-side rotors (e.g. tilt rotors) (Ref. 5).

A range of techniques for performing complex rotorcraft simulations are available which vary in their ability to predict different aspects of performance and aerodynamics (Ref. 6). Navier-Stokes simulations of complete rotorcraft configurations with fully-resolved blades are now possible (Ref. 7) and the same methods may be applied to the above-mentioned simulations. However, fully-resolved simulations come at great expense in terms of computational resources, simulation time, and manpower - particularly when multiple rotorcraft and structures are present and complex meshes must be generated. Alternative, less expensive, non-Navier-Stokes based rotor models are available, such as momentum theory methods, panel methods, and prescribed or free wake models. These models suffer variously from assumptions in their formulation that limit their applicability to certain flight states, difficulty in simulating interactions with the wakes of structures and other rotors, and/or a reliance on a priori knowledge of the rotor performance.

By coupling a rotor model with a Navier-Stokes simulation it is possible to reduce the computational expense of simulations, while still resolving the physics of the wake interactions and predicting the impact on rotorcraft performance and handling. The time-consuming task of generating a mesh for a rotor is also removed. This is achieved by substituting the resolved blades with momentum source terms equivalent to a realistic blade loading. The dependency of the blade loading on the CFD solution of the flow-field is resolved through the model which may be based on, for instance, a combination of Blade Element Theory (BET) with momentum theory or a

Presented at the AHS International 73rd Annual Forum & Technology Display, Fort Worth, Texas, USA, May 9–11, 2017.

simple lifting line approximation.

We propose an extension to the class of existing Navier-Stokes coupled rotor models known as Actuator Surface Models (ASM) by introducing a new rotor wake model to improve the prediction of the effective angle of attack along the span and thus the prediction of the loading distribution. This wake model is designed to be applied in varied operating conditions and environments, leading to a more realistic formation of the wake in the CFD solution and improved prediction of the response of the rotor to an unsteady flow-field. Three test cases have been selected for validation and comparison. The first case is a simple isolated 3D airfoil at fixed angle of attack, the second case is based on an experiment by Caradonna and Tung for a simple rotor in hover, and the third case is based on the UH-60A rotor in forward flight with rotor kinematics incorporated.

NUMERICAL METHODS

The Actuator Surface Model

The rotor models most commonly coupled with a CFD solver are actuator disc models and models based on BET, such as the virtual blade models implemented in the OpenFOAM (Ref. 8) and ANSYS Fluent (Ref. 9) CFD codes. The simple actuator disc is limited in its applicability due to the numerous simplifying assumptions in its formulation. BET based models are of greater utility since they are able to account for both radial and azimuthal variations in inflow. Typically, the inflow is either generated by an inflow model, or is directly sampled from the velocity field of the CFD solution. However, the former approach removes the coupling between the CFD solution and the rotor inflow and both approaches are strictly valid only for steady-state flow or quasi-steady flow where inflow fluctuations are at significantly lower frequency than the rotor frequency.

The concept of the Actuator Line Model (ALM) (Ref. 10) extends the BET models to unsteady simulations by representing individual blades as spanwise lines of momentum sources. In the Actuator Surface Model (ASM) (Refs. 11, 12) a chordwise distribution of momentum sources is also applied. The ALM and ASM introduce the question of how to obtain the effective angle of attack for use with 2D airfoil tables or other 2D aerodynamic model. With an unsteady flow-field there is no point in the CFD solution which will directly yield a meaningful effective angle of attack for a particular spanwise blade section. Here, a "meaningful" effective angle of attack is the angle of attack for a particular blade element that would give the same coefficients of lift and drag from the 2D airfoil table as would be observed in an experiment (or a fully-resolved simulation).

If a lifting line approximation of the blade is assumed, then an effective angle of attack may be calculated from the sum of a freestream velocity and the downwash at the quarter chord - where the freestream velocity is the incident velocity at the section, without the influence of the blade and wake. Thus, the induced velocity from the bound and wake vorticity may be used to correct the angle of attack obtained from the CFD flow-field. This requires some method to calculate the bound and wake vorticity. Corrections for the bound vorticity based on a lifting line or lifting surface representation of the blade have been used, and more recently an approximate model for the wake was shown to improve loading predictions (Ref. 12).

Our ASM utilises a lifting line blade model and a CFD convected free wake model to track the vorticity in the wake and calculate the induced velocities in complex operating conditions. The version of the free wake presented here consists of a tip vortex composed of wake markers joined by straight-line vortex filaments which are convected by the CFD velocity field. The convection of the wake markers is performed using an explicit, first-order method where the location of each marker is simply updated according to Eq. 1:

$$\mathbf{w}_i^{n+1} = \mathbf{w}_i^n + \mathbf{U}_{CFD}^n \Delta t \tag{1}$$

where $\mathbf{w}_i$ is the location of the ith wake marker, $\mathbf{U}_{CFD}$ is the velocity from the CFD computed flow-field at $\mathbf{w}_i^n$, and superscripts indicate the timestep. The circulation of the vortex filaments is determined from the peak bound circulation on the blade. The vortex cores are represented with the Scully vortex model (Ref. 13).

A schematic of the ASM for a rotor is shown in Fig. 1. The velocity field from the CFD solution is sampled ahead of each collocation point. The sample point lies on the trajectory of the collocation point and the distance between sample and collocation point is constant along the span of the blade. The sampled velocity is corrected for the bound circulation on the blade and the circulation in the wake. The 2D aerodynamics is then evaluated at each of the collocation points along the blade, taking into account the downwash from the wake, to obtain the loading and bound circulation.

Figure 2 shows the aerodynamic environment of a blade section and illustrates the method used to obtain an effective angle of attack. At sample point **s** the velocity is sampled, U_{CFD}, and the induced velocity from both the blade and the wake is calculated, $U_{in,s}$. The corrected velocity (a pseudo-freestream velocity) is obtained from:

$$U_{corr} = U_{\mathrm{CFD}} - U_{in,s} \tag{2}$$

From this corrected velocity a corrected angle of attack can be defined, α_{corr}. The downwash at the quarter-chord point, $U_{in,c}$, is then calculated and the effective velocity obtained from:

$$U_{eff} = U_{corr} + U_{in,c} \tag{3}$$

This defines an effective angle of attack, α_{eff}, which is used to interpolate the loading from 2D aerodynamic tables.

A 2D unsteady aerodynamics model has been incorporated into the ASM as the assumption of steady sectional aerodynamics is invalid in most rotor operating conditions. Beddoes' discrete-time formulation of the approximate solution

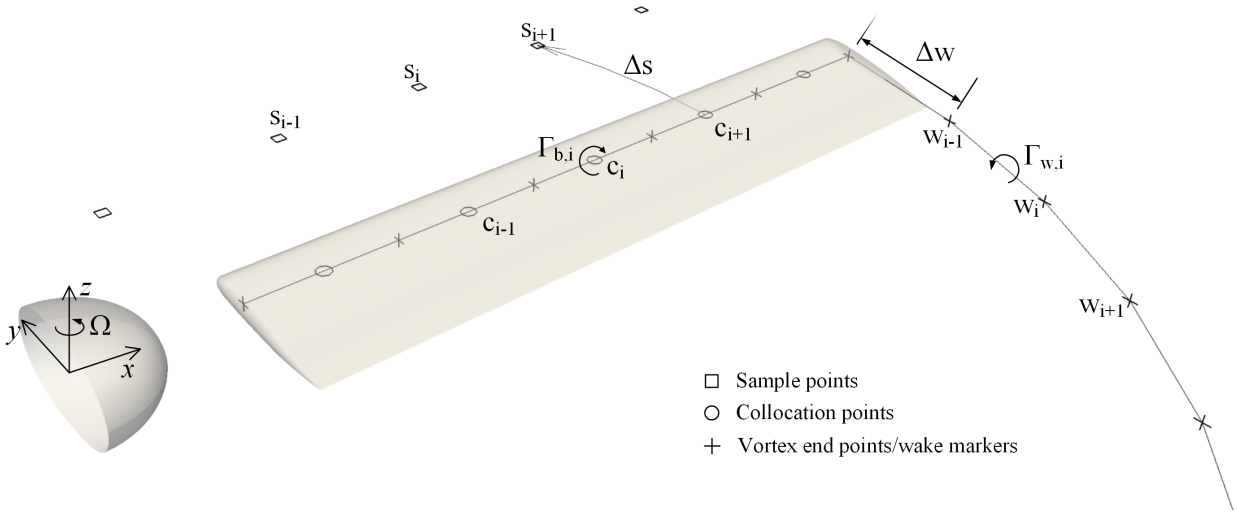

Fig. 1. Schematic showing the elements of the ASM

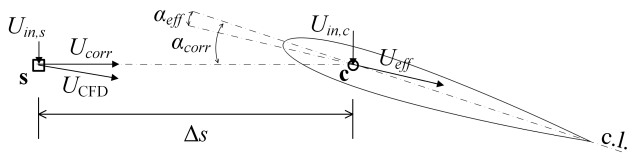

Fig. 2. Aerodynamic environment for 2D blade section.

to the indicial unsteady lift function (Ref. 14) is used here. This formulation introduces deficiency functions to represent the delay in the build-up of circulatory lift and the decay of the impulsive components. The values of these deficiency functions need only be stored for the previous time step. For the implementation in the ASM the model coefficients derived from linear aerodynamic theory were used. For full details readers are referred to Beddoes' original paper (Ref. 14). It is worth noting that this model is a predecessor to the Leishman-Beddoes dynamic stall model (Ref. 15) and is strictly valid for attached flow only.

The ASM is implemented in the framework of the OpenFOAM CFD code (Ref. 16) and demonstrated with an incompressible solver. The model is readily transferable to other codes and solvers and the method may be extended to compressible flow. The measures of success for this model will be the correlation of unsteady load predictions and wake structure with fully-resolved simulations, as well as the reduction in computational expense.

CFD Solver

The incompressible Navier-Stokes equations are solved in the simulations presented here. The assumption of incompressibility is reasonable for the low-speed wake, but is expected to introduce some discrepancy with experiments in the region of the rotor tips where the tip Mach number reaches ∼0.89 in the UH-60A test case and 0.612 in the Caradonna and Tung test case. Compressibility and Reynolds number corrections to the 2D aerodynamics tables have yet to be applied to the current model.

The solver is part of the OpenFOAM CFD code and the ASM is coupled with the PISO algorithm to advance the simulation in time. Second-order numerics are used for all temporal and spatial discretisations except in the convection of the wake markers. A multi-grid solver is applied to the pressure equation while Gauss-Seidel iteration is used for the momentum and turbulence equations. The $k-\omega$ turbulence model is used for all test cases.

TEST CASES

Isolated Wing

An isolated wing with NACA 0012 profile and aspect ratio of six at a constant 10° angle of attack and a Reynolds number of 4×10^6 was chosen to demonstrate the basic concept and validation of the ASM. The CFD convected free wake was not applied for this case in order to validate the calculation of the effective angle of attack independent of the new wake model. Instead, a simple, prescribed model is used in which a semi-infinite vortex line at the edge of each panel accounts for the trailing vorticity in the wake. The ASM in this configuration is equivalent to standard lifting line theory against which it can be validated.

A purely orthogonal mesh of 2×10^6 cells with refinement in the region of the ASM was used for this simulation. The inlet length was 20 chords, the outlet 60 chords, and the remaining boundaries were located 80 chord lengths from the wing. The wing was split into 31 bound vortices in the ASM. Figure 3

shows the mesh and the definition of the coordinate system used for this case.

Caradonna and Tung Rotor

The Caradonna and Tung case selected for this study is a two-bladed, rigid rotor with rectangular planform blades of aspect ratio six, fixed collective at 8°, and with a tip Mach number of 0.612. A NACA 0012 profile is used for the blades. The schematic in Fig. 1 shows the geometry of one half of the rotor.

Four different simulations of the Caradonna and Tung case were performed, three with the ASM and one with a resolved blade using the same numerics. In the ASM simulations the efficacy of the wake model and the validity of the CFD convected free wake were tested. To do this the ASM was run with no wake model, with a prescribed wake geometry, and with the CFD convected free wake. The prescribed wake geometry is the tip vortex trajectory for a hovering rotor from Kocurek and Tangler (Ref. 17).

Although hover cases can be formulated as steady-state simulations of a single blade (Ref. 18), these simulations were performed as fully unsteady to verify the implementation of the ASM. The dimensions of the domain were identical for all cases, with an inlet length of $5R$, outlet length of $10R$, and the boundary in the radial direction located $5R$ from the rotor. The pressure at the far-field boundaries was set by applying a constant total pressure condition. A zero gradient condition was applied to the velocity.

For the ASM simulations a simple structured mesh was generated with refinement in the wake of the rotor and the rotor disc region. A cylindrical core was removed to approximate the blockage from the hub. The mesh used for the ASM simulations contained 10×10^6 cells, while the mesh for the resolved blades contained 4×10^6 cells. Figure 4 shows the ASM mesh. The higher level of refinement for the ASM simulations was used to ensure that mesh resolution was not a factor in the results. A future study will be required to assess the mesh resolution required in the rotor disk region when using the ASM.

Rotor in Forward Flight

The UH-60A rotor is a four-bladed, fully-articulated rotor and was used as a basis for testing the ASM in forward flight. The blades have an aspect ratio of 15.5 with spanwise variation in planform and airfoil profile. Steijl et al. (Ref. 19) performed fully-resolved CFD simulations of the UH-60A rotor in high-speed forward flight with an advance ratio, μ, of 0.368 using both rigid blades and blades with prescribed elastic twist. Our test case is based on the same flight condition and trim state, detailed in Tables 1 and 2). Each hinge position in Table 1 is specified as an offset from the hub and the trim state is specified by a static displacement (β_0 and θ_0 for coning and collective respectively) and the amplitudes of the 1/rev terms of a negative Fourier series (β_c and β_s for flapping, θ_c and θ_s for cyclic).

Table 1. Forward flight hinge positions and trim state

Flap Hinge			
Offset	β_0 [°]	β_c [°]	β_s [°]
$0.0645R$	3.43	-0.7	-1.0
Pitch Hinge			
Offset	θ_0 [°]	θ_c [°]	θ_s [°]
$0.0967R$	14.6	-2.39	8.63

Table 2. Forward flight case parameters

θ_1 [$^\circ R^{-1}$]	M_{tip}	μ	α [°]
-17.3	0.89	0.368	7.31

The complex geometry of the UH-60A rotor was simplified in several ways to suit the ASM in its current state of development. The swept tip was replaced with a straight tip, the non-linear twist distribution was replaced with a linear twist (θ_1), and the lift curve for a single airfoil profile (SC1095) was used for the entire span. As it stands, with these simplifications and without corrections for Mach and Reynolds number effects, the case serves to provide qualitative validation of the ASM and the CFD convected free wake in forward flight.

The domain for the forward flight rotor has the same dimensions and structure as for the Caradonna and Tung case, except that the core of the domain is meshed (i.e. there is no blockage for the hub). The mesh is less refined than for the Caradonna and Tung, with 6×10^6 cells. Freestream boundary conditions were applied to the far-field boundaries.

RESULTS

Isolated Wing

The isolated wing at 10° angle of attack converged quickly using the ASM (less than 500 iterations to reach a residual of 10^{-6} in 35 minutes on 4 processes). Figure 5 shows the resulting flow-field and the distribution of source terms in the location of the wing. The wake of the wing forms into the familiar counter-rotating tip vortices visualised using streamlines and contours of spanwise velocity in Fig. 5.

Figure 6(a) shows the error in the angle of attack as a function of sample distance, $\Delta s/c$. The angle of attack as taken directly from the velocity field sample is shown along with the angle of attack after corrections are applied. As expected, the corrections significantly reduce the separation required between the blade and the sample point. Figure 6(b) compares the effective angle of attack along the span as calculated using the ASM, with that predicted by lifting line theory. The difference between the ASM and the lifting line results at the tip of the wing are due to the finite core radius used in the Scully vortex model (0.05 chords in this case). This result was produced using a sample offset of $1.5c$.

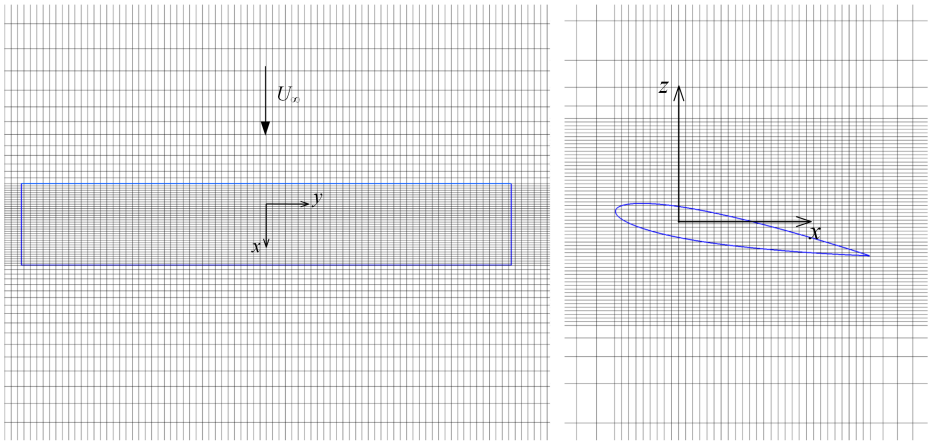

Fig. 3. Mesh and axes definition for the isolated wing.

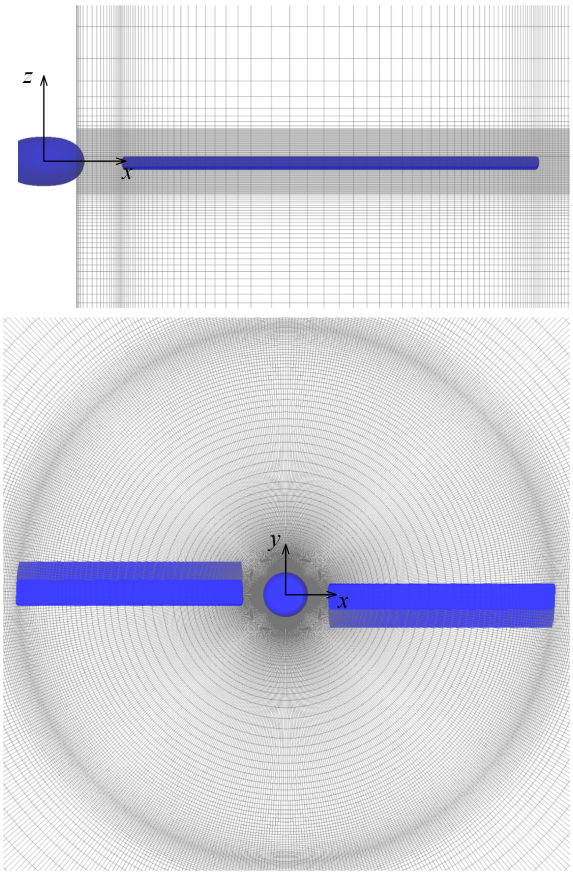

Fig. 4. Mesh for ASM simulations of the Caradonna and Tung rotor with geometry of rotor overlaid at zero azimuth.

Caradonna and Tung Rotor

Caradonna and Tung provide data for the chordwise C_p distribution at several stations along the blade. Figure 7 compares these data for stations at $r/R = 0.68$ and 0.96 with the results of the resolved blade simulation. A compressibility correction from linear theory has been applied to the C_p data from the CFD. The agreement with the Caradonna and Tung data supports the use of this relatively coarse simulation as a point of comparison for the ASM simulations.

Experimental data from Caradonna and Tung (Ref. 20) are used for comparisons of blade loading/effective angle of attack distributions (Figure 7) while the semi-empirical wake model of Kocurek and Tangler (Ref. 17) was used to generate the tip vortex geometry for comparison (Figure 9).

The objective of the ASM simulations of the Caradonna and Tung case is to verify the implementation of the ASM, demonstrate the benefit of including a wake model, and establish the validity of the CFD convected free wake. In Fig. 8 the spanwise loading distribution is shown. The loading distribution predicted by the ASM with no wake model illustrates the need for some form of wake model to calculate an effective angle of attack. Without the downwash from the wake model the effective angle of attack is over-predicted, particularly towards the tip, as there is a significant difference between the downwash at the sample point and the downwash at the quarter-chord. The loading distribution predicted by the ASM with the Kocurek and Tangler wake model is far more realistic, although the over-prediction towards the blade tip is still notable.

The loading distribution at the tip from the ASM with the CFD convected free wake is not as close to either the experimental distribution or the blade-resolved distribution as the Kocurek and Tangler model, though the results are still an improvement over the no wake simulation. The reason for this appears to lie in the sensitivity of the tip loading to the locations and orientations of the wake filaments closest to the blade tip. The convection of the wake markers leads to small differences between the actual and predicted tip vortex location. These differences are of particular importance near the tip of the blade. Constraining the tip vortex trajectory in the very near-wake may alleviate this problem.

The tip vortex trajectory was manually extracted from the resolved blade simulation by visualising Q-criterion. Figure 9 contains a plot of this trajectory as contraction ratio (r/R) and descent ratio (z/R) as a function of wake age. The trajectories from both the prescribed Kocurek and Tangler model and the CFD convected free wake model are also plotted in Fig.

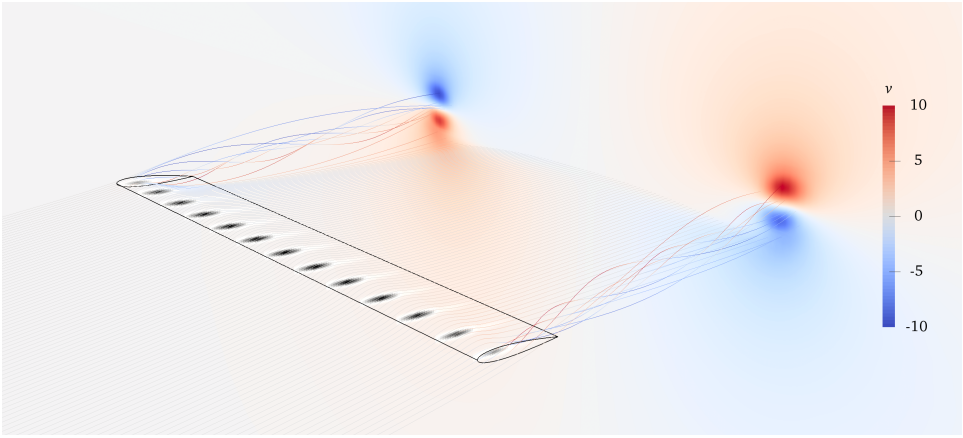

Fig. 5. Flow-field calculated using the ASM for a NACA 0012 wing with aspect ratio 6 at 10° angle of attack. Slices through airfoil show distribution of source terms, the plane in the wake is located 5 chord lengths downstream of the quarter-chord line and is coloured by spanwise velocity, v, as are the streamlines.

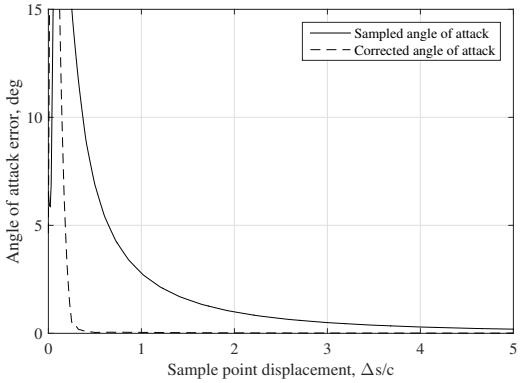

(a) Error in angle of attack as a function of sample point displacement

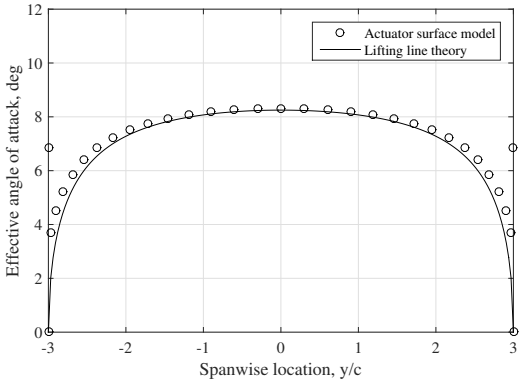

(b) Effective angle of attack distribution along span

Fig. 6. Angle of attack correction and effective angle of attack predictions from the ASM.

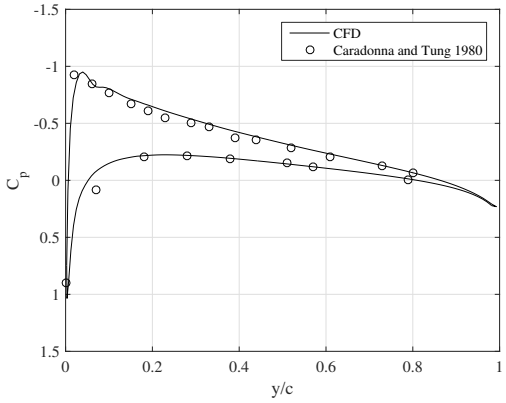

(a) $r/R = 0.68$

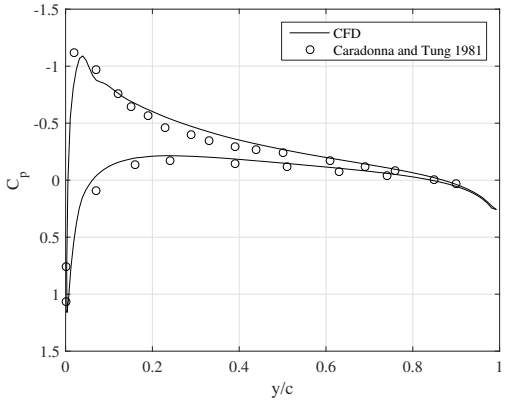

(b) $r/R = 0.96$

Fig. 7. Chordwise C_p distribution at two sections along blade – experimental (Ref. 20) and CFD data.

9. The correlation of the new wake model with the resolved blade CFD and the prescribed model suggests that the premise of the CFD convected free wake is sound. The jitter in the trajectory is likely a product of the first-order, explicit numerics used here.

Table 3 contains the coefficient of thrust values obtained from the different CFD simulations as well as the experimental value. The coefficient of thrust from the resolved simulation is distinctly lower than the experimental value, the reason for which is the under-prediction of thrust at the rotor tip, as is apparent in Fig. 8. As expected, the ASM without a wake

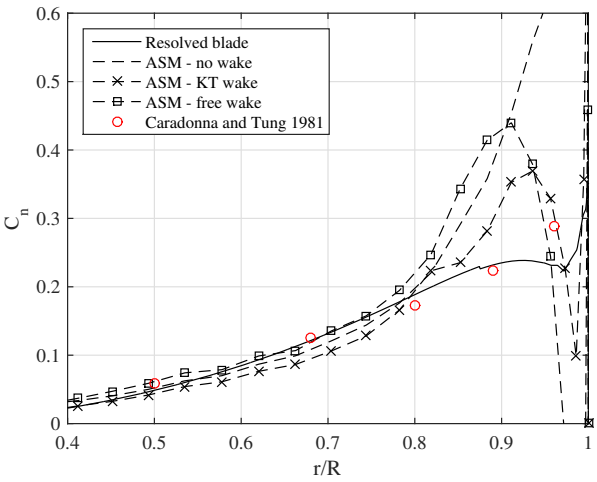

Fig. 8. Spanwise loading distribution – comparison of different ASM wake models with experimental data and resolved CFD.

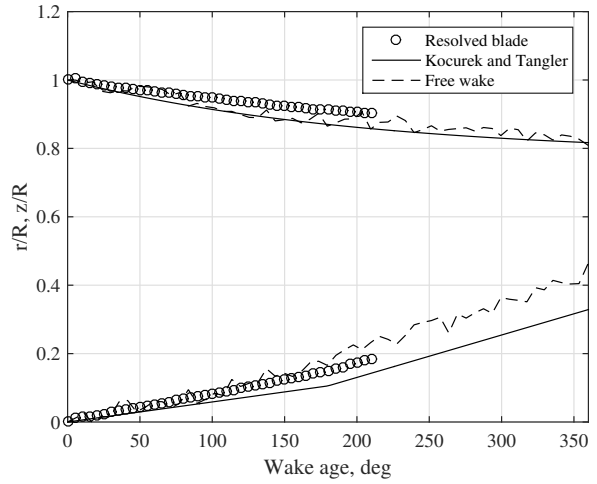

Fig. 9. Tip vortex location in terms of radial (r/R, decreasing with wake age) and axial (z/R, increasing with wake age) coordinates as a function of wake age from the Kocurek and Tangler model, the CFD convected free wake, and from the resolved blade CFD.

model over-predicts the thrust coefficient significantly, while both wake models obtain similar results within 10% of the experimental value.

Table 3. Thrust coefficient for Caradonna and Tung rotor at 8° collective

Method	Thrust Coefficient
Experiment	0.0105
Resolved blade	0.0091
No wake	0.0136
KT wake	0.0098
Free wake	0.0096

The near-wake flow-field generated by the ASM is visualised in Fig. 10 alongside that from the resolved blade simulation. The ASM with no wake model and with the Kocurek and Tangler wake model produce similar wake structures while the higher wake resolution in the ASM simulations is evident when compared to the resolved blade simulation.

A comprehensive study of the computational savings from the ASM has not been performed, though a preliminary comparison with the resolved simulation can be made. The fully-resolved simulation required approximately 300 CPU seconds per iteration to compute with a 4 million cell mesh while the ASM simulation required approximately 520 CPU seconds per iteration on a 10 million cell mesh. Taking into account the difference in mesh size, the speed per iteration of the method was not significantly faster in these simulations. However, the stable time step size that could be achieved using the ASM was much greater (5 to 10 times), leading to proportionally shorter computational times while achieving substantially higher resolution in the wake.

Rotor in Forward Flight

Figure 11 shows the normal force coefficient at three different stations along the blade as a function of azimuth angle (where the zero azimuth direction is aligned with the freestream velocity). The results from the ASM simulations with no wake and with the CFD convected free wake are compared to data from the fully-resolved simulations Steijl et al. (Ref. 19). There is good qualitative agreement between the fully-resolved simulation and the ASM simulations. The simplifications made to the geometry of the case mean that quantitative agreement is not expected.

At approximately 70° azimuth there is a large disturbance in the ASM results, this is the product of a near-pass of the tip vortex from the preceding blade. Smaller peaks at the same azimuth in the fully-resolved simulations indicate that the timing of this blade vortex passage is correct, but either the separation between vortex and blade is smaller in the ASM simulations, or the response of the 2D unsteady aerodynamics model is too sensitive. Another, less prominent vortex passage is visible around 325°.

A prescribed wake model formulated by Beddoes for rotors in forward flight (Ref. 21) was run with the parameters of the rotor case to obtain a tip vortex trajectory for comparison. The contraction ratio from this model is plotted alongside the contraction ratio from the free wake model in Fig. 12.

CONCLUSIONS

The fully CFD-coupled ASM and wake model presented in this paper are at an early stage of development. In this paper we sought to outline the method and demonstrate the validity of the concept. To this end we applied the ASM to a steady-state, finite aspect ratio wing, a simple rotor in hover, and a more realistic rotor in forward flight. The results from the steady-state wing verified the implementation

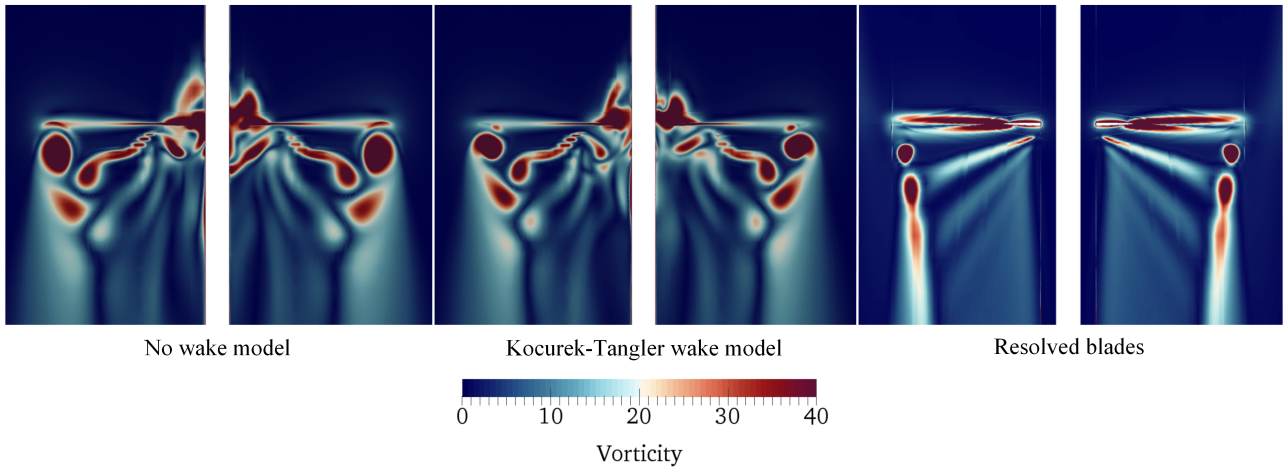

Fig. 10. Vorticity contours in the wake of the Caradonna and Tung rotor from the ASM with and without a wake model and the resolved simulation.

of the model as well as the efficacy of the corrections to the sampled velocity field. The hovering Caradonna and Tung rotor (Ref. 20) provided comparisons with experimental data and a blade-resolved CFD simulation. The inclusion of a wake model was shown to improve predictions of load distribution and thrust coefficient and the CFD convected free wake was shown to generate a wake geometry very similar to both the blade-resolved CFD and Kocurek and Tangler's prescribed wake model (Ref. 17). Favourable results were obtained from the UH-60A case, especially considering the simplifications made. The azimuthal loading correlated well with results from the blade-resolved calculations of Steijl et al. (Ref. 19) and free wake trajectory agreed with the trajectory predicted by Beddoes' prescribed wake model (Ref. 21).

While these results are encouraging these cases have also highlighted areas for further development of this ASM. The spanwise loading distribution for the Caradonna and Tung case was not completely satisfactory. The difference between the ASM with the free wake and the ASM with the Kocurek and Tangler wake model can likely be ascribed to small perturbations in the wake geometry near the tip due to the convection of the free wake. The remaining discrepancy between the ASM tip loading and the experimental data requires further investigation, the first line of which will be the inclusion of a model for the outboard vortex sheet. The tip vortex trajectory predicted by the CFD convected free wake followed the expected trend, but the jitter in the trajectory highlights the need for improved convection numerics. In the forward flight case there were prominent excursions from the data of Steijl et al. where the blade passed close to a tip vortex. Improving the response to these interactions as well as the overall comparison will require the extension of the ASM to handle the complex geometry of the UH-60A rotor as well as a review of the 2D unsteady aerodynamics. Lastly, the high Mach number of the UH-60A case makes prominent the need to implement compressibility corrections along with Reynolds number corrections.

ACKNOWLEDGMENTS

The authors would like to thank the Australian Defence Science and Technology Group for providing funding and support for this work. The authors also acknowledge the University of Sydney HPC service at The University of Sydney for providing HPC resources that have contributed to the research results reported within this paper.

REFERENCES

[1]Oruc, I., Joseph, F., Jeremy, S., and Rajiv, S., "Coupled Flight Dynamics and CFD Simulations of Rotorcraft/Terrain Interactions," AIAA Modeling and Simulation Technologies Conference, San Diego, Jan. 2016.

[2]Forsythe, J., Lynch, E., and Polsky, S., "Coupled Flight Simulator and CFD Calculations of Ship Airwake using HPCMP CREATE-AV Kestrel," 53rd AIAA Aerospace Sciences Meeting, Kissimmee, Jan. 2015.

[3]Soneson, G., Horn, J., and Zheng, A., "Simulation Testing of Advanced Response Types for Ship-Based Rotorcraft," *Journal of the American Helicopter Society*, Vol. 61, (3), 2016.

[4]Zhang, J., Smith, E., and Zajaczkowski, F., "Analysis of Start-Up and Shutdown of Rotor in Complex Wind Conditions on Sea-Based Oil Rig," 5th Decennial AHS Aeromechanics Specialist's Conference, San Francisco, Jan. 2014.

[5]Narducci, R., Jiang, F., Liu, J., and Clark, R., "CFD Modeling of Tiltrotor Shipboard Aerodynamics with Rotor Wake Interactions," 27th AIAA Applied Aerodynamics Conference, San Antonio, Jun. 2009.

[6]Conlisk, A., "Modern Helicopter Rotor Aerodynamics," *Progress in Aerospace Sciences*, Vol. 27, (5), 2001.

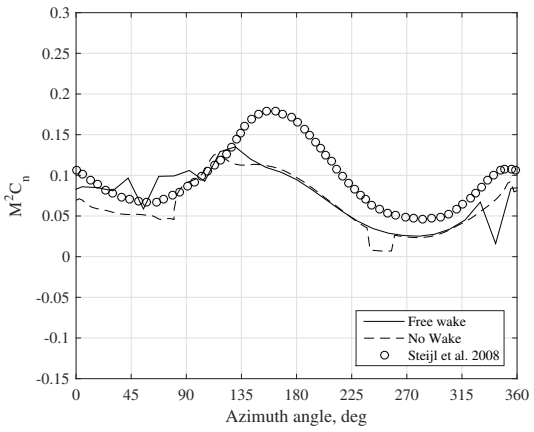

(a) $r/R = 0.675$

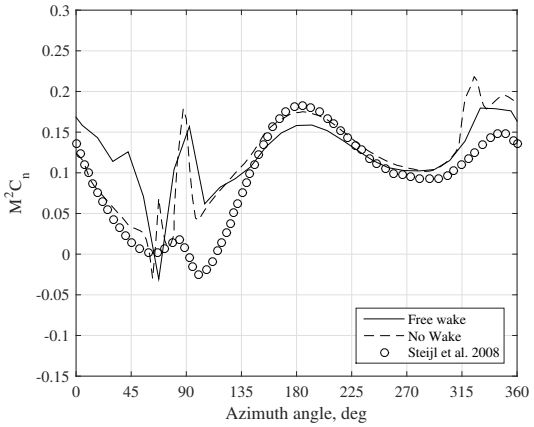

(b) $r/R = 0.865$

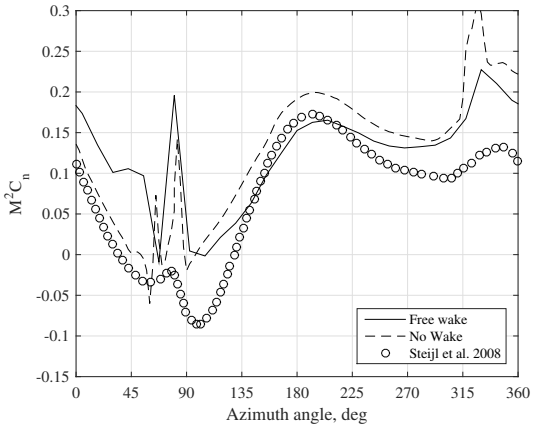

(c) $r/R = 0.920$

Fig. 11. Normal force (M^2C_n) as a function of azimuth angle at various r/R stations. Results are shown for simulations using the CFD convected free wake and no wake model, these are compared to results from resolved simulations performed by Steijl et al. (Ref. 19)

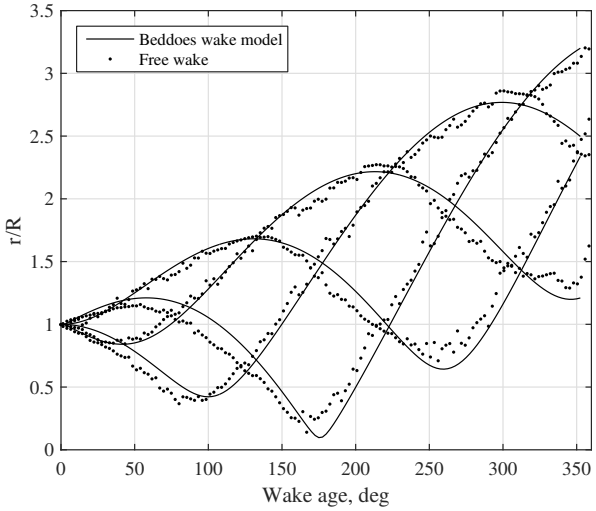

Fig. 12. Contraction ratio (r/R) for all four tip vortices from Beddoes' prescribed wake model (Ref. 21) and the free wake.

ments for Helicopter Flows," *Aerospace Science and Technology*, Vol. 19, (1), 2012.

[8]Wahono, S., "Development of Virtual Blade Model for Modelling Helicopter Rotor Downwash in OpenFOAM," TR 2931, Australian Defence Science Technology Group, 2013.

[9]Ruith, M., "Unstructured, Multiplex Rotor Source Model with Thrust and Moment Trimming - Fluent's VBM Model," 23rd AIAA Applied Aerodynamics Conference, Toronto, Jun. 2005.

[10]Sorensen, J. and Shen, W., "Numerical Modeling of Wind Turbine Wakes," *Journal of Fluids Engineering*, Vol. 124, (2), 2002.

[11]Shen, W., Zhang, J., and Sorensen, J., "The Actuator Surface Model: A New Navier-Stokes Based Model for Rotor Computations," *Journal of Solar Energy Engineering*, Vol. 131, (1), 2009.

[12]Kim, T., Oh, S., and Yee, K., "Improved Actuator Surface Method for Wind Turbine Applications," *Renewable Energy*, Vol. 76, 2015.

[13]Scully, M., *Computation of Helicotper Rotor Wake Geometry and its influence on Rotor Harmonic Airloads*, Ph.D. thesis, Massachusetts Institute of Technology, 1975.

[14]Beddoes, T., "Practical Computation of Unsteady Lift," *Vertica*, Vol. 8, (1), 1984.

[15]Leishman, J. and Beddoes, T., "A Semi-Empirical Model for Dynamic Stall," *Journal of the American Helicopter Society*, Vol. 34, (3), 1989.

[16]CFD Direct, "OpenFOAM - Open Source Computational Fluid Dynamics," http://cfd.direct/openfoam/, Sep. 2016.

[17]Kocurek, J. and Tangler, J., "A Prescribed Wake Lifting Surface Hover Performance Analysis," *Journal of the American Helicopter Society*, Vol. 22, (1), 1977.

[18]Garcia, A. and Barakos, G., "Hover Predictions of the S-76 Rotor using HMB2 – Model to Full Scale," 54th AIAA Aerospace Sciences Meeting, San Diego, Jan. 2016.

[19]Steijl, R., Barakos, G., and Badcock, K., "Computational Study of the Advancing-Side Lift-Phase Problem," *Journal of Aircraft*, Vol. 45, (1), 2008.

[20]Caradonna, F. and Tung, C., "Experimental and Analytical Studies of a Model Helicopter Rotor in Hover," TM 81232, NASA, 1981.

[21]Beddoes, T., "A Wake Model for High Resolution Airloads," First International Conference on Rotorcraft Basic Research, Feb. 1985.